

Measurement of the Absolute Branching Fraction of $D_s^+ \rightarrow \tau^+ \nu_\tau$ via $\tau^+ \rightarrow e^+ \nu_e \bar{\nu}_\tau$

M. Ablikim¹, M. N. Achasov^{10,c}, P. Adlarson⁶⁷, S. Ahmed¹⁵, M. Albrecht⁴, R. Aliberti²⁸, A. Amoroso^{66A,66C}, M. R. An³², Q. An^{63,49}, X. H. Bai⁵⁷, Y. Bai⁴⁸, O. Bakina²⁹, R. Baldini Ferroli^{23A}, I. Balossino^{24A}, Y. Ban^{38,j}, K. Begzsuren²⁶, N. Berger²⁸, M. Bertani^{23A}, D. Bettoni^{24A}, F. Bianchi^{66A,66C}, J. Bloms⁶⁰, A. Bortone^{66A,66C}, I. Boyko²⁹, R. A. Briere⁵, H. Cai⁶⁸, X. Cai^{1,49}, A. Calcaterra^{23A}, G. F. Cao^{1,54}, N. Cao^{1,54}, S. A. Cetin^{53A}, J. F. Chang^{1,49}, W. L. Chang^{1,54}, G. Chelkov^{29,b}, D. Y. Chen⁶, G. Chen¹, H. S. Chen^{1,54}, M. L. Chen^{1,49}, S. J. Chen³⁵, X. R. Chen²⁵, Y. B. Chen^{1,49}, Z. J. Chen^{20,k}, W. S. Cheng^{66C}, G. Cibinetto^{24A}, F. Cossio^{66C}, X. F. Cui³⁶, H. L. Dai^{1,49}, X. C. Dai^{1,54}, A. Dbeyssi¹⁵, R. E. de Boer⁴, D. Dedovich²⁹, Z. Y. Deng¹, A. Denig²⁸, I. Denysenko²⁹, M. Destefanis^{66A,66C}, F. De Mori^{66A,66C}, Y. Ding³³, C. Dong³⁶, J. Dong^{1,49}, L. Y. Dong^{1,54}, M. Y. Dong^{1,49,54}, X. Dong⁶⁸, S. X. Du⁷¹, Y. L. Fan⁶⁸, J. Fang^{1,49}, S. S. Fang^{1,54}, Y. Fang¹, R. Farinelli^{24A}, L. Fava^{66B,66C}, F. Feldbauer⁴, G. Felici^{23A}, C. Q. Feng^{63,49}, J. H. Feng⁵⁰, M. Fritsch⁴, C. D. Fu¹, Y. Gao^{63,49}, Y. Gao^{38,j}, Y. Gao⁶⁴, Y. G. Gao⁶, I. Garzia^{24A,24B}, P. T. Ge⁶⁸, C. Geng⁵⁰, E. M. Gersabeck⁵⁸, A. Gilman⁶¹, K. Goetzen¹¹, L. Gong³³, W. X. Gong^{1,49}, W. Gradl²⁸, M. Greco^{66A,66C}, L. M. Gu³⁵, M. H. Gu^{1,49}, S. Gu², Y. T. Gu¹³, C. Y. Guan^{1,54}, A. Q. Guo²², L. B. Guo³⁴, R. P. Guo⁴⁰, Y. P. Guo^{9,h}, A. Guskov^{29,b}, T. T. Han⁴¹, W. Y. Han³², X. Q. Hao¹⁶, F. A. Harris⁵⁶, K. L. He^{1,54}, F. H. Heinsius⁴, C. H. Heinz²⁸, T. Held⁴, Y. K. Heng^{1,49,54}, C. Herold⁵¹, M. Himmelreich^{11,f}, T. Holtmann⁴, G. Y. Hou^{1,54}, Y. R. Hou⁵⁴, Z. L. Hou¹, H. M. Hu^{1,54}, J. F. Hu^{47,l}, T. Hu^{1,49,54}, Y. Hu¹, G. S. Huang^{63,49}, L. Q. Huang⁶⁴, X. T. Huang⁴¹, Y. P. Huang¹, Z. Huang^{38,j}, T. Hussain⁶⁵, N. Hüsken^{22,28}, W. Ikegami Andersson⁶⁷, W. Imoehl²², M. Irshad^{63,49}, S. Jaeger⁴, S. Janchiv²⁶, Q. Ji¹, Q. P. Ji¹⁶, X. B. Ji^{1,54}, X. L. Ji^{1,49}, Y. Y. Ji⁴¹, H. B. Jiang⁴¹, X. S. Jiang^{1,49,54}, J. B. Jiao⁴¹, Z. Jiao¹⁸, S. Jin³⁵, Y. Jin⁵⁷, M. Q. Jing^{1,54}, T. Johansson⁶⁷, N. Kalantar-Nayestanaki⁵⁵, X. S. Kang³³, R. Kappert⁵⁵, M. Kavatsyuk⁵⁵, B. C. Ke^{43,1}, I. K. Keshk⁴, A. Khoukaz⁶⁰, P. Kiese²⁸, R. Kiuchi¹, R. Kliemt¹¹, L. Koch³⁰, O. B. Kolcu^{53A,e}, B. Kopf⁴, M. Kuemmel⁴, M. Kuessner⁴, A. Kupsc⁶⁷, M. G. Kurth^{1,54}, W. Kühn³⁰, J. J. Lane⁵⁸, J. S. Lange³⁰, P. Larin¹⁵, A. Lavania²¹, L. Lavezzi^{66A,66C}, Z. H. Lei^{63,49}, H. Leithoff²⁸, M. Lellmann²⁸, T. Lenz²⁸, C. Li³⁹, C. H. Li³², Cheng Li^{63,49}, D. M. Li⁷¹, F. Li^{1,49}, G. Li¹, H. Li⁴³, H. Li^{63,49}, H. B. Li^{1,54}, H. J. Li¹⁶, J. L. Li⁴¹, J. Q. Li⁴, J. S. Li⁵⁰, Ke Li¹, L. K. Li¹, Lei Li³, P. R. Li^{31,m,n}, S. Y. Li⁵², W. D. Li^{1,54}, W. G. Li¹, X. H. Li^{63,49}, X. L. Li⁴¹, Xiaoyu Li^{1,54}, Z. Y. Li⁵⁰, H. Liang^{63,49}, H. Liang^{1,54}, H. Liang²⁷, Y. F. Liang⁴⁵, Y. T. Liang²⁵, G. R. Liao¹², L. Z. Liao^{1,54}, J. Libby²¹, C. X. Lin⁵⁰, B. J. Liu⁵⁴, C. X. Liu¹, D. Liu^{15,63}, F. H. Liu⁴⁴, Fang Liu¹, Feng Liu⁶, H. B. Liu¹³, H. M. Liu^{1,54}, Huanhuan Liu¹, Huihui Liu¹⁷, J. B. Liu^{63,49}, J. L. Liu⁶⁴, J. Y. Liu^{1,54}, K. Liu¹, K. Y. Liu³³, L. Liu^{63,49}, M. H. Liu^{9,h}, P. L. Liu¹, Q. Liu⁵⁴, Q. Liu⁶⁸, S. B. Liu^{63,49}, Shuai Liu⁴⁶, T. Liu^{1,54}, W. M. Liu^{63,49}, X. Liu^{31,m,n}, Y. Liu^{31,m,n}, Y. B. Liu³⁶, Z. A. Liu^{1,49,54}, Z. Q. Liu⁴¹, X. C. Lou^{1,49,54}, F. X. Lu⁵⁰, H. J. Lu¹⁸, J. D. Lu^{1,54}, J. G. Lu^{1,49}, X. L. Lu¹, Y. Lu¹, Y. P. Lu^{1,49}, C. L. Luo³⁴, M. X. Luo⁷⁰, P. W. Luo⁵⁰, T. Luo^{9,h}, X. L. Luo^{1,49}, X. R. Lyu⁵⁴, F. C. Ma³³, H. L. Ma¹, L. L. Ma⁴¹, M. M. Ma^{1,54}, Q. M. Ma¹, R. Q. Ma^{1,54}, R. T. Ma⁵⁴, X. X. Ma^{1,54}, X. Y. Ma^{1,49}, F. E. Maas¹⁵, M. Maggiora^{66A,66C}, S. Maldaner⁴, S. Malde⁶¹, A. Mangoni^{23B}, Y. J. Mao^{38,j}, Z. P. Mao¹, S. Marcello^{66A,66C}, Z. X. Meng⁵⁷, J. G. Messchendorp⁵⁵, G. Mezzadri^{24A}, T. J. Min³⁵, R. E. Mitchell²², X. H. Mo^{1,49,54}, Y. J. Mo⁶, N. Y. Muchnoi^{10,c}, H. Muramatsu⁵⁹, S. Nakhoul^{11,f}, Y. Nefedov²⁹, F. Nerling^{11,f}, I. B. Nikolaev^{10,c}, Z. Ning^{1,49}, S. Nisar^{8,i}, S. L. Olsen⁵⁴, Q. Ouyang^{1,49,54}, S. Pacetti^{23B,23C}, X. Pan^{9,h}, Y. Pan⁵⁸, A. Pathak¹, P. Patteri^{23A}, M. Pelizaeus⁴, H. P. Peng^{63,49}, K. Peters^{11,f}, J. Pettersson⁶⁷, J. L. Ping³⁴, R. G. Ping^{1,54}, R. Poling⁵⁹, V. Prasad^{63,49}, H. Qi^{63,49}, H. R. Qi⁵², K. H. Qi²⁵, M. Qi³⁵, T. Y. Qi⁹, S. Qian^{1,49}, W. B. Qian⁵⁴, Z. Qian⁵⁰, C. F. Qiao⁵⁴, L. Q. Qin¹², X. P. Qin⁹, X. S. Qin⁴¹, Z. H. Qin^{1,49}, J. F. Qiu¹, S. Q. Qu³⁶, K. H. Rashid⁶⁵, K. Ravindran²¹, C. F. Redmer²⁸, A. Rivetti^{66C}, V. Rodin⁵⁵, M. Rolo^{66C}, G. Rong^{1,54}, Ch. Rosner¹⁵, M. Rump⁶⁰, H. S. Sang⁶³, A. Sarantsev^{29,d}, Y. Schelhaas²⁸, C. Schnier⁴, K. Schoenning⁶⁷, M. Scodreggio^{24A,24B}, D. C. Shan⁴⁶, W. Shan¹⁹, X. Y. Shan^{63,49}, J. F. Shangguan⁴⁶, M. Shao^{63,49}, C. P. Shen⁹, H. F. Shen^{1,54}, P. X. Shen³⁶, X. Y. Shen^{1,54}, H. C. Shi^{63,49}, R. S. Shi^{1,54}, X. Shi^{1,49}, X. D. Shi^{63,49}, J. J. Song⁴¹, W. M. Song^{27,1}, Y. X. Song^{38,j}, S. Soso^{66A,66C}, S. Spataro^{66A,66C}, K. X. Su⁶⁸, P. P. Su⁴⁶, F. F. Sui⁴¹, G. X. Sun¹, H. K. Sun¹, J. F. Sun¹⁶, L. Sun⁶⁸, S. S. Sun^{1,54}, T. Sun^{1,54}, W. Y. Sun²⁷, W. Y. Sun³⁴, X. Sun^{20,k}, Y. J. Sun^{63,49}, Y. K. Sun^{63,49}, Y. Z. Sun¹, Z. T. Sun¹, Y. H. Tan⁶⁸, Y. X. Tan^{63,49}, C. J. Tang⁴⁵, G. Y. Tang¹, J. Tang⁵⁰, J. X. Teng^{63,49}, V. Thoren⁶⁷, W. H. Tian⁴³, Y. T. Tian²⁵, I. Uman^{53B}, B. Wang¹, C. W. Wang³⁵, D. Y. Wang^{38,j}, H. J. Wang^{31,m,n}, H. P. Wang^{1,54}, K. Wang^{1,49}, L. L. Wang¹, M. Wang⁴¹, M. Z. Wang^{38,j}, Meng Wang^{1,54}, W. Wang⁵⁰, W. H. Wang⁶⁸, W. P. Wang^{63,49}, X. Wang^{38,j}, X. F. Wang^{31,m,n}, X. L. Wang^{9,h}, Y. Wang^{63,49}, Y. Wang⁵⁰, Y. D. Wang³⁷, Y. F. Wang^{1,49,54}, Y. Q. Wang¹, Y. Y. Wang^{31,m,n}, Z. Wang^{1,49}, Z. Y. Wang¹, Ziyi Wang⁵⁴, Zongyuan Wang^{1,54}, D. H. Wei¹², F. Weidner⁶⁰, S. P. Wen¹, D. J. White⁵⁸, U. Wiedner⁴, G. Wilkinson⁶¹, M. Wolke⁶⁷, L. Wollenberg⁴, J. F. Wu^{1,54}, L. H. Wu¹, L. J. Wu^{1,54}, X. Wu^{9,h}, Z. Wu^{1,49}, L. Xia^{63,49}, H. Xiao^{9,h}, S. Y. Xiao¹, Z. J. Xiao³⁴, X. H. Xie^{38,j}, Y. G. Xie^{1,49}, Y. H. Xie⁶, T. Y. Xing^{1,54}, G. F. Xu¹, Q. J. Xu¹⁴, W. Xu^{1,54}, X. P. Xu⁴⁶, Y. C. Xu⁵⁴, F. Yan^{9,h}, L. Yan^{9,h}, W. B. Yan^{63,49}, W. C. Yan⁷¹, Xu Yan⁴⁶, H. J. Yang^{42,g}, H. X. Yang¹, L. Yang⁴³, S. L. Yang⁵⁴, Y. X. Yang¹², Yifan Yang^{1,54}, Zhi Yang²⁵, M. Ye^{1,49}, M. H. Ye⁷, J. H. Yin¹, Z. Y. You⁵⁰, B. X. Yu^{1,49,54}, C. X. Yu³⁶, G. Yu^{1,54}, J. S. Yu^{20,k}, T. Yu⁶⁴, C. Z. Yuan^{1,54}, L. Yuan², X. Q. Yuan^{38,j}, Y. Yuan¹, Z. Y. Yuan⁵⁰, C. X. Yue³², A. Yuncu^{53A,a}, A. A. Zafar⁶⁵, Zeng⁶, Y. Zeng^{20,k}, A. Q. Zhang¹, B. X. Zhang¹, Guangyi Zhang¹⁶, H. Zhang⁶³, H. H. Zhang²⁷, H. H. Zhang⁵⁰, H. Y. Zhang^{1,49}, J. J. Zhang⁴³, J. L. Zhang⁶⁹, J. Q. Zhang³⁴, J. W. Zhang^{1,49,54}, J. Y. Zhang¹, J. Z. Zhang^{1,54}, Jianyu Zhang^{1,54}, Jiawei Zhang^{1,54}, L. M. Zhang⁵², L. Q. Zhang⁵⁰, Lei Zhang³⁵, S. Zhang⁵⁰, S. F. Zhang³⁵, Shulei Zhang^{20,k}, X. D. Zhang³⁷, X. Y. Zhang⁴¹, Y. Zhang⁶¹, Y. H. Zhang^{1,49}, Y. T. Zhang^{63,49}, Yan Zhang^{63,49}, Yao Zhang¹, Yi Zhang^{9,h}, Z. H. Zhang⁶, Z. Y. Zhang⁶⁸, G. Zhao¹, J. Zhao³², J. Y. Zhao^{1,54}, J. Z. Zhao^{1,49}, Lei Zhao^{63,49}, Ling Zhao¹, M. G. Zhao³⁶, Q. Zhao¹, S. J. Zhao⁷¹, Y. B. Zhao^{1,49}, Y. X. Zhao²⁵, Z. G. Zhao^{63,49}, A. Zhemchugov^{29,b}, B. Zheng⁶⁴, J. P. Zheng^{1,49}, Y. Zheng^{38,j}, Y. H. Zheng⁵⁴, B. Zhong³⁴, C. Zhong⁶⁴, L. P. Zhou^{1,54}, Q. Zhou^{1,54}, X. Zhou⁶⁸, X. K. Zhou⁵⁴, X. R. Zhou^{63,49}, X. Y. Zhou³², A. N. Zhu^{1,54}, J. Zhu³⁶, K. Zhu¹, K. J. Zhu^{1,49,54}, S. H. Zhu⁶², T. J. Zhu⁶⁹, W. J. Zhu^{9,h}, W. J. Zhu³⁶, Y. C. Zhu^{63,49}, Z. A. Zhu^{1,54}, B. S. Zou¹, J. H. Zou¹

(BESIII Collaboration)

- ¹ Institute of High Energy Physics, Beijing 100049, People's Republic of China
- ² Beihang University, Beijing 100191, People's Republic of China
- ³ Beijing Institute of Petrochemical Technology, Beijing 102617, People's Republic of China
- ⁴ Bochum Ruhr-University, D-44780 Bochum, Germany
- ⁵ Carnegie Mellon University, Pittsburgh, Pennsylvania 15213, USA
- ⁶ Central China Normal University, Wuhan 430079, People's Republic of China
- ⁷ China Center of Advanced Science and Technology, Beijing 100190, People's Republic of China
- ⁸ COMSATS University Islamabad, Lahore Campus, Defence Road, Off Raiwind Road, 54000 Lahore, Pakistan
- ⁹ Fudan University, Shanghai 200443, People's Republic of China
- ¹⁰ G.I. Budker Institute of Nuclear Physics SB RAS (BINP), Novosibirsk 630090, Russia
- ¹¹ GSI Helmholtzcentre for Heavy Ion Research GmbH, D-64291 Darmstadt, Germany
- ¹² Guangxi Normal University, Guilin 541004, People's Republic of China
- ¹³ Guangxi University, Nanning 530004, People's Republic of China
- ¹⁴ Hangzhou Normal University, Hangzhou 310036, People's Republic of China
- ¹⁵ Helmholtz Institute Mainz, Staudinger Weg 18, D-55099 Mainz, Germany
- ¹⁶ Henan Normal University, Xinxiang 453007, People's Republic of China
- ¹⁷ Henan University of Science and Technology, Luoyang 471003, People's Republic of China
- ¹⁸ Huangshan College, Huangshan 245000, People's Republic of China
- ¹⁹ Hunan Normal University, Changsha 410081, People's Republic of China
- ²⁰ Hunan University, Changsha 410082, People's Republic of China
- ²¹ Indian Institute of Technology Madras, Chennai 600036, India
- ²² Indiana University, Bloomington, Indiana 47405, USA
- ²³ INFN Laboratori Nazionali di Frascati, (A)INFN Laboratori Nazionali di Frascati, I-00044, Frascati, Italy; (B)INFN Sezione di Perugia, I-06100, Perugia, Italy; (C)University of Perugia, I-06100, Perugia, Italy
- ²⁴ INFN Sezione di Ferrara, (A)INFN Sezione di Ferrara, I-44122, Ferrara, Italy; (B)University of Ferrara, I-44122, Ferrara, Italy
- ²⁵ Institute of Modern Physics, Lanzhou 730000, People's Republic of China
- ²⁶ Institute of Physics and Technology, Peace Ave. 54B, Ulaanbaatar 13330, Mongolia
- ²⁷ Jilin University, Changchun 130012, People's Republic of China
- ²⁸ Johannes Gutenberg University of Mainz, Johann-Joachim-Becher-Weg 45, D-55099 Mainz, Germany
- ²⁹ Joint Institute for Nuclear Research, 141980 Dubna, Moscow region, Russia
- ³⁰ Justus-Liebig-Universitaet Giessen, II. Physikalisches Institut, Heinrich-Buff-Ring 16, D-35392 Giessen, Germany
- ³¹ Lanzhou University, Lanzhou 730000, People's Republic of China
- ³² Liaoning Normal University, Dalian 116029, People's Republic of China
- ³³ Liaoning University, Shenyang 110036, People's Republic of China
- ³⁴ Nanjing Normal University, Nanjing 210023, People's Republic of China
- ³⁵ Nanjing University, Nanjing 210093, People's Republic of China
- ³⁶ Nankai University, Tianjin 300071, People's Republic of China
- ³⁷ North China Electric Power University, Beijing 102206, People's Republic of China
- ³⁸ Peking University, Beijing 100871, People's Republic of China
- ³⁹ Qufu Normal University, Qufu 273165, People's Republic of China
- ⁴⁰ Shandong Normal University, Jinan 250014, People's Republic of China
- ⁴¹ Shandong University, Jinan 250100, People's Republic of China
- ⁴² Shanghai Jiao Tong University, Shanghai 200240, People's Republic of China
- ⁴³ Shanxi Normal University, Linfen 041004, People's Republic of China
- ⁴⁴ Shanxi University, Taiyuan 030006, People's Republic of China
- ⁴⁵ Sichuan University, Chengdu 610064, People's Republic of China
- ⁴⁶ Soochow University, Suzhou 215006, People's Republic of China
- ⁴⁷ South China Normal University, Guangzhou 510006, People's Republic of China
- ⁴⁸ Southeast University, Nanjing 211100, People's Republic of China
- ⁴⁹ State Key Laboratory of Particle Detection and Electronics, Beijing 100049, Hefei 230026, People's Republic of China
- ⁵⁰ Sun Yat-Sen University, Guangzhou 510275, People's Republic of China
- ⁵¹ Suranaree University of Technology, University Avenue 111, Nakhon Ratchasima 30000, Thailand
- ⁵² Tsinghua University, Beijing 100084, People's Republic of China
- ⁵³ Turkish Accelerator Center Particle Factory Group, (A)Istanbul Bilgi University, 34060 Eyup, Istanbul, Turkey; (B)Near East University, Nicosia, North Cyprus, Mersin 10, Turkey
- ⁵⁴ University of Chinese Academy of Sciences, Beijing 100049, People's Republic of China
- ⁵⁵ University of Groningen, NL-9747 AA Groningen, The Netherlands
- ⁵⁶ University of Hawaii, Honolulu, Hawaii 96822, USA
- ⁵⁷ University of Jinan, Jinan 250022, People's Republic of China
- ⁵⁸ University of Manchester, Oxford Road, Manchester, M13 9PL, United Kingdom
- ⁵⁹ University of Minnesota, Minneapolis, Minnesota 55455, USA

⁶⁰ University of Muenster, Wilhelm-Klemm-Str. 9, 48149 Muenster, Germany

⁶¹ University of Oxford, Keble Rd, Oxford, UK OX13RH

⁶² University of Science and Technology Liaoning, Anshan 114051, People's Republic of China

⁶³ University of Science and Technology of China, Hefei 230026, People's Republic of China

⁶⁴ University of South China, Hengyang 421001, People's Republic of China

⁶⁵ University of the Punjab, Lahore-54590, Pakistan

⁶⁶ University of Turin and INFN, (A)University of Turin, I-10125, Turin, Italy; (B)University of Eastern Piedmont, I-15121, Alessandria, Italy; (C)INFN, I-10125, Turin, Italy

⁶⁷ Uppsala University, Box 516, SE-75120 Uppsala, Sweden

⁶⁸ Wuhan University, Wuhan 430072, People's Republic of China

⁶⁹ Xinyang Normal University, Xinyang 464000, People's Republic of China

⁷⁰ Zhejiang University, Hangzhou 310027, People's Republic of China

⁷¹ Zhengzhou University, Zhengzhou 450001, People's Republic of China

^a Also at Bogazici University, 34342 Istanbul, Turkey

^b Also at the Moscow Institute of Physics and Technology, Moscow 141700, Russia

^c Also at the Novosibirsk State University, Novosibirsk, 630090, Russia

^d Also at the NRC "Kurchatov Institute", PNPI, 188300, Gatchina, Russia

^e Also at Istanbul Arel University, 34295 Istanbul, Turkey

^f Also at Goethe University Frankfurt, 60323 Frankfurt am Main, Germany

^g Also at Key Laboratory for Particle Physics, Astrophysics and Cosmology, Ministry of Education; Shanghai Key Laboratory for Particle Physics and Cosmology; Institute of Nuclear and Particle Physics, Shanghai 200240, People's Republic of China

^h Also at Key Laboratory of Nuclear Physics and Ion-beam Application (MOE) and Institute of Modern Physics, Fudan University, Shanghai 200443, People's Republic of China

ⁱ Also at Harvard University, Department of Physics, Cambridge, MA, 02138, USA

^j Also at State Key Laboratory of Nuclear Physics and Technology, Peking University, Beijing 100871, People's Republic of China

^k Also at School of Physics and Electronics, Hunan University, Changsha 410082, China

^l Also at Guangdong Provincial Key Laboratory of Nuclear Science, Institute of Quantum Matter, South China Normal University, Guangzhou 510006, China

^m Also at Frontiers Science Center for Rare Isotopes, Lanzhou University, Lanzhou 730000, People's Republic of China

ⁿ Also at Lanzhou Center for Theoretical Physics, Lanzhou University, Lanzhou 730000, People's Republic of China

Using a data set of 6.32 fb^{-1} of e^+e^- annihilation data collected with the BESIII detector at center-of-mass energies between 4178 and 4226 MeV, we have measured the absolute branching fraction of the leptonic decay $D_s^+ \rightarrow \tau^+\nu_\tau$ via $\tau^+ \rightarrow e^+\nu_e\bar{\nu}_\tau$ to be $\mathcal{B}_{D_s^+ \rightarrow \tau^+\nu_\tau} = (5.27 \pm 0.10 \pm 0.12) \times 10^{-2}$, where the first uncertainty is statistical and the second is systematic. Combining with $f_{D_s^+}$ from Lattice quantum chromodynamics calculations or the $|V_{cs}|$ from the CKMfitter group, we extract $|V_{cs}| = 0.978 \pm 0.009 \pm 0.012$ and $f_{D_s^+} = (251.1 \pm 2.4 \pm 3.0) \text{ MeV}$, respectively. These results are the most precise to date. Combining our result with the world averages of $\mathcal{B}_{D_s^+ \rightarrow \tau^+\nu_\tau}$ and $\mathcal{B}_{D_s^+ \rightarrow \mu^+\nu_\mu}$, we obtain the ratio of the branching fractions $\mathcal{B}_{D_s^+ \rightarrow \tau^+\nu_\tau}/\mathcal{B}_{D_s^+ \rightarrow \mu^+\nu_\mu} = 9.72 \pm 0.37$, which is consistent with the standard model prediction of lepton flavor universality.

PACS numbers: 13.20.Fc, 14.40.Lb

Leptonic decays of charged pseudoscalar mesons can provide accurate determinations of Cabibbo-Kobayashi-Maskawa (CKM) matrix elements and a clean setting for tests of the lepton flavor universality (LFU). In the standard model (SM), the partial decay width of $D_s^+ \rightarrow l^+\nu_l$ ($l = e, \mu, \tau$) to the lowest order is given by [1]

$$\Gamma_{D_s^+ \rightarrow l^+\nu_l} = \frac{G_F^2 f_{D_s^+}^2 m_{D_s^+}^3}{8\pi} |V_{cs}|^2 \mu_l^2 (1 - \mu_l^2)^2, \quad (1)$$

where G_F is the Fermi coupling constant, $f_{D_s^+}$ is the decay constant parameterizing strong-interaction effects between the two initial-state quarks, V_{cs} is the $c \rightarrow s$ CKM matrix element, and μ_l is the ratio of the l^+ lepton mass to the D_s^+ meson mass, $m_{D_s^+}$.

From Eq. (1), it is clear that the ratio of the decay

widths $\Gamma_{D_s^+ \rightarrow \tau^+\nu_\tau}/\Gamma_{D_s^+ \rightarrow \mu^+\nu_\mu}$ only depends on μ_τ and μ_μ , and is equal to 9.75 ± 0.01 [2]. This is consistent with the experimental measurements [2] given the current relatively large uncertainties. In recent years, some hints of LFU violation in semileptonic B decays have been reported by different experiments [3–7]. In Ref. [8], it is argued that the violation may occur in $c \rightarrow s$ transitions due to the interference between the SM amplitude involving a W^+ boson and the amplitude including a charged Higgs boson in a two-Higgs-doublet model. To test LFU in D decays, measurements of the $D_s^+ \rightarrow l^+\nu_l$ decays with improved precision are required.

Given $f_{D_s^+}$ from Lattice quantum chromodynamics (LQCD) calculations [9], a precision measurement of the

branching fraction (BF) of $D_s^+ \rightarrow l^+ \nu_l$ ($\mathcal{B}_{D_s^+ \rightarrow l^+ \nu_l}$) allows an accurate determination of $|V_{cs}|$ and a stringent test of the unitarity of the CKM matrix. Conversely, given $|V_{cs}|$ from the SM global fit [2], the $\mathcal{B}_{D_s^+ \rightarrow l^+ \nu_l}$ value allows one to extract $f_{D_s^+}$ and verify the theoretical determinations of the decay constant.

Previous measurements of $\mathcal{B}_{D_s^+ \rightarrow \tau^+ \nu_\tau}$ from CLEO [10–13], BABAR [14], Belle [15], and BESIII [16–18] have limited precision. In this Letter, we report a significantly improved measurement using the $\tau^+ \rightarrow e^+ \nu_e \bar{\nu}_\tau$ decay [19], benefiting from larger and cleaner data samples. The data samples used, corresponding to a total integrated luminosity of 6.32 fb^{-1} , were collected at center-of-mass energies (E_{cm}) of 4178, 4189, 4199, 4209, 4219, and around 4226 MeV [20, 21] with the BESIII detector [22, 23] operating at the BEPCII collider [24].

Simulated data samples produced with a GEANT4-based [25] Monte Carlo (MC) package, which incorporates the geometric description of the BESIII detector and the detector response, are used to determine detection efficiencies and to estimate backgrounds. The MC simulation includes the beam-energy spread and initial-state radiation (ISR). Moreover, one combined “cocktail” MC sample corresponding to 40 times the integrated luminosity of data is produced, including the production of open-charm final states, ISR production of vector charmonium states, and continuum processes. Details can be found in Ref. [17].

We apply a “double-tag” (DT) technique [26, 27] to select the leptonic D_s^+ decays. Events of $e^+e^- \rightarrow D_s^{*+} (\rightarrow \gamma/\pi^0 D_s^+) D_s^-$ and $e^+e^- \rightarrow (\gamma_{\text{ISR}}) D_s^+ D_s^-$ are identified by fully reconstructing a hadronic D_s^- decay (“single tag” or “ST”) from eleven decay modes: $K_S^0 K^-$, $K^+ K^- \pi^-$, $K^+ K^- \pi^- \pi^0$, $K_S^0 K^- \pi^+ \pi^-$, $K_S^0 K^+ \pi^- \pi^-$, $\pi^+ \pi^- \pi^-$, $\pi^- \eta$, $\pi^- \pi^0 \eta$, $\pi^- \eta'_{\pi^+ \pi^- \eta}$, $\pi^- \eta'_{\gamma \rho^0}$, and $K^- \pi^+ \pi^-$, of which $K_S^0 \rightarrow \pi^+ \pi^-$, $\pi^0(\eta) \rightarrow \gamma\gamma$, $\eta'_{\pi^+ \pi^- \eta} \rightarrow \pi^+ \pi^- \eta$, $\eta'_{\gamma \rho^0} \rightarrow \gamma \rho^0$, and $\rho^0 \rightarrow \pi^+ \pi^-$, respectively. A DT signal event consists of an ST D_s^- candidate accompanied by a $D_s^+ \rightarrow \tau^+ \nu_\tau$ signal candidate.

The absolute $\mathcal{B}_{D_s^+ \rightarrow l^+ \nu_l}$ is given by

$$\mathcal{B}_{D_s^+ \rightarrow \tau^+ \nu_\tau} = \frac{N_{\text{DT}}/\epsilon_{\text{DT}}}{\sum_i (N_{\text{ST}}^i/\epsilon_{\text{ST}}^i) \mathcal{B}_{\tau^+ \rightarrow e^+ \nu_e \bar{\nu}_\tau}}, \quad (2)$$

where i indicates the data samples at the six energy points, N_{ST}^i (N_{DT}) and ϵ_{ST}^i (ϵ_{DT}) are the ST (DT) yields and efficiencies, and $\mathcal{B}_{\tau^+ \rightarrow e^+ \nu_e \bar{\nu}_\tau}$ is the world average BF of $\tau^+ \rightarrow e^+ \nu_e \bar{\nu}_\tau$ [2]. The ST yields N_{ST}^i are obtained for each energy point, while the DT yield N_{DT} is obtained for the combined data sample because of limited statistics.

The ST D_s^- candidates are reconstructed from the above eleven hadronic decay modes with almost the same selection criteria as those in Ref. [28], the differences are described here. For $D_s^- \rightarrow K_S^0 K^-$, the K_S^0 candidate is not required to have a decay length larger than twice the vertex resolution. For $D_s^- \rightarrow \pi^+ \pi^- \pi^-$, the

K_S^0 candidates are retained in the invariant mass of either $\pi^+ \pi^-$ combination. The specific ionization energy loss (dE/dx) in the main drift chamber (MDC) and the time-of-flight (TOF) information are combined and used for particle identification (PID) by forming confidence levels for the charged pion and kaon hypotheses (CL_π , CL_K). Kaons are identified by requiring $CL_K > CL_\pi$, while pions except for those from K_S^0 decays are demanded to satisfy $CL_\pi > CL_K$. To suppress background from Bhabha events, the relative-probability sum, $\sum_{j=1}^n \frac{CL_\pi^j}{CL_\pi^j + CL_K^j + CL_e^j}$, must be smaller than 2.0 (0.9) for $n > 1$ ($n = 1$), where n is the number of charged tracks for the ST mode.

The recoil mass against the tag D_s^- , $M_{\text{rec}} = \sqrt{(E_{\text{cm}} - \sqrt{|\vec{p}_{D_s^-}^-|^2 + m_{D_s^-}^2})^2 - |\vec{p}_{D_s^-}^-|^2}$, is used to select the $e^+e^- \rightarrow (\gamma_{\text{ISR}}) D_s^{(*)\pm} D_s^\mp$ events, where $\vec{p}_{D_s^-}$ is the momentum of the reconstructed D_s^- and $m_{D_s^-}$ is the D_s^- nominal mass. Events with M_{rec} lying within the mass windows of [2.050, 2.195], [2.048, 2.205], [2.046, 2.215], [2.044, 2.225], [2.042, 2.235], and [2.040, 2.220] GeV/ c^2 are retained for further analysis for the data samples at $E_{\text{cm}} = 4178, 4189, 4199, 4209, 4219$, and around 4226 MeV, respectively. At most one tag D_s^- candidate per tag mode per charge is selected in each event. In case of multiple candidates, the one with the minimum $|M_{\text{rec}} - m_{D_s^*}|$ is chosen, where $m_{D_s^*}$ is the nominal D_s^* mass [2].

The ST yields are obtained from fits to the invariant mass spectra of the ST D_s^- candidates (M_{ST}). In the fits, the D_s^- signal is modeled by the MC-simulated shape convolved with a Gaussian resolution function. The combinatorial background is described by a first to third order Chebychev function. For $D_s^- \rightarrow K_S^0 K^-$, the peaking background from $D^- \rightarrow K_S^0 \pi^-$ is incorporated with the MC-simulated shape and its yield is left free. The fit results for the data sample at $E_{\text{cm}} = 4178$ MeV are shown in Fig. 1 as an example. For each tag mode, the ST yield is obtained within a tag-dependent M_{ST} window corresponding to approximately $\pm 3\sigma$ of the D_s mass. Following the same procedure, the ST efficiencies are estimated using the cocktail MC sample. Table I lists the sum (R) of the ratios of the ST yield over the ST efficiency from the six data samples.

In the presence of the ST D_s^- candidate, we select the signal candidate for $D_s^+ \rightarrow \tau^+ \nu_\tau$ with $\tau^+ \rightarrow e^+ \nu_e \bar{\nu}_\tau$. Given the very small variation of detection efficiencies and backgrounds at different energy points, the six data samples are combined for further analysis. The DT candidates are required to have exactly one charged track in addition to the daughters of the tag side and that track must have a charge opposite that of the tag side decay. The track is also required to be associated with a good electromagnetic calorimeter (EMC) shower, as described in Ref. [28]. To identify the positron, the combined dE/dx , TOF, and EMC information is used to de-

TABLE I. The ratios of the ST yield in data over the ST efficiency summed over the six data samples ($R = \sum_i \frac{N_{DT}^{i, \text{ST}}}{\epsilon_{ST}^i}$), the numbers of DT events (N_{DT}^{tot}), the numbers of backgrounds of non- D_s^- , $D_s^+ \rightarrow K_L^0 e^+ \nu_e$, and $D_s^+ \rightarrow X e^+ \nu_e$ in the $E_{\text{extra}}^{\text{tot}} < 0.4$ GeV signal region ($N_{DT}^{\text{non-}D_s^-}$, $N_{DT}^{K_L^0 e^+ \nu_e}$, and $N_{DT}^{X e^+ \nu_e}$), the numbers of DT events after removing backgrounds (N_{DT}), the DT efficiencies (ϵ_{DT}), and the obtained $\mathcal{B}_{D_s^+ \rightarrow \tau^+ \nu_\tau}$. Both ϵ_{ST}^i in R and ϵ_{DT} include the relevant BF's for K_S^0 , π^0 , η , η' , and ρ^0 decays. The $N_{DT}^{K_L^0 e^+ \nu_e}$ is fixed in the fit and its uncertainty will be treated later as a systematic uncertainty. For $\mathcal{B}_{D_s^+ \rightarrow \tau^+ \nu_\tau}$, the first, second, and third uncertainties are statistical, tag-mode dependent systematic and tag-mode independent systematic, respectively. The statistical uncertainty from the ST yield in R is included in the second uncertainty of $\mathcal{B}_{D_s^+ \rightarrow \tau^+ \nu_\tau}$. For the other numbers, the uncertainties are statistical only.

Mode	$R(\times 10^4)$	N_{DT}^{tot}	$N_{DT}^{\text{non-}D_s^-}$	$N_{DT}^{K_L^0 e^+ \nu_e}$	$N_{DT}^{X e^+ \nu_e}$	N_{DT}	ϵ_{DT} (%)	$\mathcal{B}_{D_s^+ \rightarrow \tau^+ \nu_\tau}$ (%)
$K_S^0 K^-$	17.5	500 ± 22	30.2 ± 2.9	60	56.9 ± 2.7	353 ± 23	23.69 ± 0.22	$4.79 \pm 0.31 \pm 0.07 \pm 0.11$
$K^+ K^- \pi^-$	62.7	2394 ± 49	544.5 ± 15.0	154	202.8 ± 5.0	1493 ± 51	26.63 ± 0.13	$5.03 \pm 0.17 \pm 0.04 \pm 0.11$
$K^+ K^- \pi^- \pi^0$	69.5	1198 ± 35	386.1 ± 9.5	55	92.2 ± 5.5	664 ± 36	9.52 ± 0.08	$5.64 \pm 0.31 \pm 0.17 \pm 0.12$
$K_S^0 K^- \pi^+ \pi^-$	11.3	203 ± 14	82.2 ± 5.1	9	14.8 ± 2.0	97 ± 15	8.51 ± 0.22	$5.68 \pm 0.90 \pm 0.23 \pm 0.13$
$K_S^0 K^+ \pi^- \pi^-$	18.5	291 ± 17	59.1 ± 4.4	16	26.6 ± 2.4	189 ± 18	9.95 ± 0.15	$5.78 \pm 0.54 \pm 0.13 \pm 0.13$
$\pi^+ \pi^- \pi^-$	13.7	952 ± 31	323.3 ± 12.0	49	70.7 ± 3.8	509 ± 33	38.39 ± 0.37	$5.43 \pm 0.36 \pm 0.13 \pm 0.12$
$\pi^- \eta$	19.1	359 ± 19	32.1 ± 3.8	23	40.4 ± 2.1	264 ± 19	12.93 ± 0.15	$6.00 \pm 0.44 \pm 0.22 \pm 0.13$
$\pi^- \pi^0 \eta$	105.9	1065 ± 33	229.1 ± 7.9	65	100.8 ± 5.2	670 ± 34	6.65 ± 0.05	$5.35 \pm 0.27 \pm 0.19 \pm 0.12$
$\pi^- \eta'_{\pi^+ \pi^-} \eta$	43.6	167 ± 13	1.0 ± 0.3	11	17.7 ± 1.4	137 ± 13	2.56 ± 0.04	$6.93 \pm 0.66 \pm 0.17 \pm 0.15$
$\pi^- \eta'_{\rho^0} \rho^0$	47.3	478 ± 22	92.0 ± 5.6	32	53.3 ± 3.2	301 ± 23	7.21 ± 0.08	$4.96 \pm 0.38 \pm 0.14 \pm 0.11$
$K^- \pi^+ \pi^-$	7.2	787 ± 28	466.3 ± 14.6	22	35.2 ± 3.5	263 ± 32	34.45 ± 0.69	$5.96 \pm 0.72 \pm 0.25 \pm 0.13$

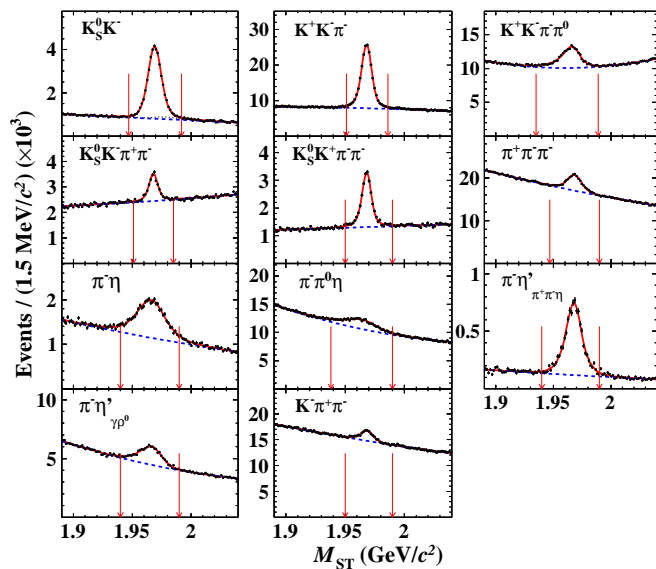


FIG. 1. Fits to the M_{ST} distributions of the ST D_s^- candidates for the data sample at $E_{\text{cm}} = 4178$ MeV. Dots with error bars are data, solid red lines are the total fits, dashed blue lines are the combinatorial backgrounds, and dotted black line for $D_s^- \rightarrow K_S^0 K^-$ is from the $D^- \rightarrow K_S^0 \pi^- \pi^-$ background. The pairs of arrows denote the signal regions.

termine a CL_e . We assign the track as a positron if it satisfies $CL_e > 0.1\%$ and $CL_e / (CL_e + CL_\pi + CL_K) > 0.8$. The candidate track is further required to have a momentum in the MDC greater than 0.2 GeV/c and a ratio

of the energy deposited in the EMC to the momentum greater than 0.8 .

To effectively discriminate signal from background, we adopt the variable $E_{\text{extra}}^{\text{tot}}$ following Refs. [10, 11]. It is the total energy of the good isolated EMC showers, excluding those associated with the ST selection and those within 5° of the initial direction of the positron. The latter eliminates energy associated with final state radiation (FSR) from the positron track. We do not exclude soft photons or π^0 's originating directly from the D_s^* . The $E_{\text{extra}}^{\text{tot}}$ distributions of the DT candidates for various tag modes in the combined data sample are shown in Fig. 2. Entries in the lowest bin correspond to those events without any extra good EMC showers. Signal events accumulate below 0.4 GeV in $E_{\text{extra}}^{\text{tot}}$. We determine the background yield by a fit to the region $E_{\text{extra}}^{\text{tot}} > 0.6$ GeV, where the signal is negligible, and extrapolate the backgrounds into the signal region using MC-derived shapes. The signal yield is then determined in the region $E_{\text{extra}}^{\text{tot}} < 0.4$ GeV by statistically subtracting the expected backgrounds from the DT events seen in data. This procedure is insensitive to the signal shape, except for the inefficiency introduced by the definition of the signal region.

The backgrounds in the $E_{\text{extra}}^{\text{tot}}$ distributions can be divided into three categories. The first one is the non- D_s^- background with an incorrectly reconstructed ST D_s^- . The second is the $D_s^+ \rightarrow K_L^0 e^+ \nu_e$ background, which survives when the K_L^0 passes through the detector without decaying or significantly interacting. The third is the $D_s^+ \rightarrow X e^+ \nu_e$ background, which is dominated by the six semileptonic decays $D_s^+ \rightarrow \eta e^+ \nu_e$, $\eta' e^+ \nu_e$, $\phi e^+ \nu_e$, $f_0(980) e^+ \nu_e$, $K^*(892)^0 e^+ \nu_e$, and $K_S^0 e^+ \nu_e$. The latter two

cases are dominated by correctly reconstructed ST D_s^- .

A binned maximum likelihood fits are performed in the region $E_{\text{extra}}^{\text{tot}} > 0.6$ GeV. The shape and size of the non- D_s^- background are fully specified with the events in the M_{ST} sideband regions ([1.895, 1.92] and [2.01, 2.035] GeV/ c^2). For the tag modes with neutral daughters, the resolution difference between data and MC simulation (called data-MC difference) has been corrected. The shape of the $D_s^+ \rightarrow K_L^0 e^+ \nu_e$ background is modeled by the MC-derived shape corrected by a two dimensional (polar angle and momentum) data-MC difference for the K_L^0 detector response. These correction factors are obtained by using a control sample of $D^0 \rightarrow K_L^0 \pi^+ \pi^-$ from 2.93 fb $^{-1}$ of data collected at $E_{\text{cm}} = 3.773$ GeV [29]. The background yield is calculated with $\mathcal{B}_{D_s^+ \rightarrow K^0 e^+ \nu_e} = (3.25 \pm 0.38 \pm 0.16) \times 10^{-3}$, quoted from our previous work [30]. The peaking background from $D^- \rightarrow K_S^0 \pi^-$ is present only for the $D_s^- \rightarrow K_S^0 K^-$ tag mode and its yield is estimated from the M_{ST} fit. The yield of the $D_s^+ \rightarrow X e^+ \nu_e$ background is left free, with the shape extracted from the MC simulation with the individual BFs for the six background channels fixed as $\mathcal{B}_{D_s^+ \rightarrow \eta e^+ \nu_e} = (2.32 \pm 0.08)\%$ [31–33], $\mathcal{B}_{D_s^+ \rightarrow \eta' e^+ \nu_e} = (0.80 \pm 0.07)\%$ [31–33], $\mathcal{B}_{D_s^+ \rightarrow \phi e^+ \nu_e} = (2.37 \pm 0.11)\%$ [33–35], $\mathcal{B}_{D_s^+ \rightarrow f_0(980) e^+ \nu_e}, f_0(980) \rightarrow \pi\pi = (0.30 \pm 0.05)\%$ [36, 37], $\mathcal{B}_{D_s^+ \rightarrow K^*(892)^0 e^+ \nu_e} = (0.21 \pm 0.03)\%$ [30, 33], and $\mathcal{B}_{D_s^+ \rightarrow K^0 e^+ \nu_e} = (0.34 \pm 0.04)\%$ [30, 33]. Moreover, the MC-based shapes have been further weighted by the individual ST yields at various energy points.

Table I lists the obtained DT yields and DT efficiencies, where the latter are evaluated from the cocktail MC sample with same steps.

In the BF measurement, most uncertainties related to the ST selection are cancelled. The remaining systematic uncertainties are divided into two cases. The first case is from tag-mode dependent systematic uncertainties.

Systematic uncertainties in the ST yield is examined by changing the fit range, the signal and background shapes, and the bin size and the background fluctuation of the fitted ST yield. The alternative fit range is chosen as [1.895, 2.035] GeV/ c^2 . The nominal signal shapes obtained from the cocktail MC sample are replaced with those from the signal MC sample. The background shape is changed to a different order of the Chebychev function. The bin size is doubled. The differences in the ratio of the ST yield over the ST efficiency for a given ST mode for all variations, and the background fluctuation of the fitted ST yield, are weighted by the ST yields in various data samples, and added in quadrature. The resulting overall systematic uncertainty of the ST yield is 0.61%.

Tag bias related to the ST selection arises from different event environments (e.g., charged and neutral multiplicities). The ratios of the ST efficiencies from the cocktail MC sample and the signal MC sample for various tag modes are examined. The difference between the

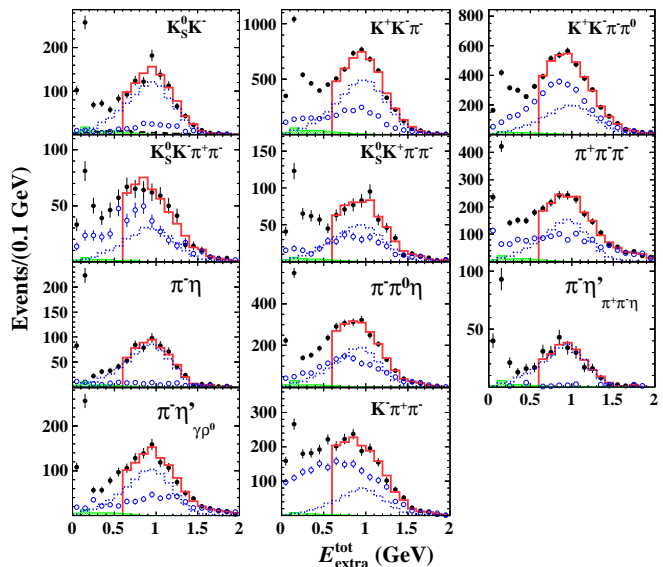


FIG. 2. The $E_{\text{extra}}^{\text{tot}}$ distributions of the DT candidates in the combined data sample (black points with error bars), along with results of fits to $E_{\text{extra}}^{\text{tot}} > 0.6$ GeV (solid red) and background estimates for non- D_s^- (circles with error bars), $D_s^+ \rightarrow K_L^0 e^+ \nu_e$ (hatched green), $D_s^+ \rightarrow X e^+ \nu_e$ (dotted blue), and $D^- \rightarrow K_S^0 \pi^-$ (dashed black, only for $D_s^- \rightarrow K_S^0 K^-$).

two ST efficiencies is weighted by the ST yields in various data samples. The systematic uncertainty due to tag bias is assigned to be 0.26%.

For the non- D_s^- background, we replace the distributions from the M_{ST} sidebands with those for the background events in the M_{ST} signal region from the cocktail MC. The change of the measured BF, 0.07%, is assigned as the systematic uncertainty. In the nominal fit, the MC-based correction signal events in the M_{ST} sideband regions are normalized using the ratio of signal yields in the M_{ST} distributions of data and the cocktail MC sample. Alternative fits are performed 10^4 times with the ratio varied according to a random Gaussian sampling based on its statistical error. The distribution of the relative difference on the DT yield is fitted by a Gaussian function, and the width of 0.07% is taken as the systematic uncertainty. Here, and below where this method is also used, no significant biases in the means are observed. The systematic uncertainty from the $D^- \rightarrow K_S^0 \pi^-$ background for the $D_s^- \rightarrow K_S^0 K^-$ tag mode is assigned to be 0.05% with a similar technique. The uncertainty from the limited MC statistics is 0.31%. The quadratic sum of all the tag-mode dependent systematic uncertainties is 0.74%.

The second case is from tag-mode independent systematic uncertainties. The systematic uncertainty associated with the $E_{\text{extra}}^{\text{tot}} < 0.4$ GeV signal region is estimated using the DT events of $D_s^+ \rightarrow \pi^+(\pi^0)\eta$. The efficiencies for

the $E_{\text{extra}}^{\text{tot}} < 0.4$ requirement in the control sample have been verified to be consistent with those in our signal decay. The associated systematic uncertainty is assigned to be 1.0%.

The systematic uncertainty related to extra charged tracks is studied with the DT events of $D_s^+ \rightarrow \pi^+ \phi (\rightarrow K^+ K^-)$ and $D_s^+ \rightarrow K^+ \bar{K}^* (892)^0 (\rightarrow K^- \pi^+)$. The data-MC difference of the efficiencies, 1.4%, is taken as the systematic uncertainty.

The systematic uncertainties associated with the e^+ tracking [37] and PID efficiencies are studied with a control sample of radiative Bhabha events. The two dimensional (momentum and the polar angle) efficiencies in the control sample are re-weighted to match those in our signal decay. The re-weighted data-MC difference on e^+ tracking (PID) efficiency, 0.3% (0.3%), is assigned as the relevant systematic uncertainty.

The systematic uncertainty from the shape of $D_s^+ \rightarrow K_L^0 e^+ \nu_e$ background is estimated by replacing the corrected shape of $E_{\text{extra}}^{\text{tot}}$ with the uncorrected one. The change of the measured BF is negligible. We also examine the size of the $D_s^+ \rightarrow K_L^0 e^+ \nu_e$ background by sampling the quoted BF [30] 10^4 times based on a Gaussian distribution given by its uncertainty. The width of the relative difference of the fitted DT yield, 1.2%, is assigned as the systematic uncertainty.

The uncertainty coming from the fixed $D_s^+ \rightarrow X e^+ \nu_e$ background shape is examined by varying the proportion of each of the six main background modes via sampling their BFs [30–37] 10^4 times, based on Gaussian distributions given by their uncertainties. The width of the relative difference of the DT efficiency, weighted by the ST yields in various data samples, 0.1%, is taken as the systematic uncertainty.

The uncertainty due to FSR effect is checked with radiative Bhabha events. The data-MC difference of the efficiencies for the requirement of including FSR photons, 0.5%, is taken as the systematic uncertainty. The uncertainty from the quoted BF for $\tau^+ \rightarrow e^+ \nu_e \bar{\nu}_\tau$ is 0.2% [2]. The quadratic sum of all tag-mode independent systematic uncertainties is 2.2%.

The last column of Table I lists the obtained $\mathcal{B}_{D_s^+ \rightarrow \tau^+ \nu_\tau}$ for various tag modes. Weighting them by the inverse squares of the combined statistical and tag-mode dependent systematic uncertainties, we obtain $\mathcal{B}_{D_s^+ \rightarrow \tau^+ \nu_\tau} = (5.27 \pm 0.10 \pm 0.12) \times 10^{-2}$. Here, the first error is statistical, and the second is the quadrature sum of the tag-mode dependent (0.040×10^{-2}) and independent (0.117×10^{-2}) systematic uncertainties. Combining Eq. (1) with $\mathcal{B}_{D_s^+ \rightarrow \tau^+ \nu_\tau} = \tau_{D_s^+} \Gamma_{D_s^+ \rightarrow \tau^+ \nu_\tau}$, where $\tau_{D_s^+}$ is the D_s^+ lifetime [2], we find $f_{D_s^+} |V_{cs}| = (244.4 \pm 2.3 \pm 2.9)$ MeV. With $|V_{cs}| = 0.97320 \pm 0.00011$ from the CKMfitter group [2], we obtain $f_{D_s^+} = (251.1 \pm 2.4 \pm 3.0)$ MeV. Alternatively, taking $f_{D_s^+} = (249.9 \pm 0.5)$ MeV from LQCD calculations [9], we determine $|V_{cs}| = 0.978 \pm 0.009 \pm 0.012$.

Based on our result of $f_{D_s^+} |V_{cs}|$ and the measured $f_{D^+} |V_{cd}|$ in Ref. [38], along with $|V_{cd}/V_{cs}| = 0.23259 \pm 0.00049$ from the SM global fit [2], it yields $f_{D_s^+}/f_{D^+} = 1.244 \pm 0.017 \pm 0.021$, which is consistent with the LQCD calculation [9] within 2.4σ . Alternatively, taking $f_{D_s^+}/f_{D^+} = 1.1783 \pm 0.0016$ calculated by LQCD [9] as input, we extract $|V_{cd}/V_{cs}|^2 = 0.049 \pm 0.001 \pm 0.002$, which agrees with the value obtained from the CKM fitter within 2.3σ .

Combining our measured BF, the world average value [2] of $\mathcal{B}_{D_s^+ \rightarrow \tau^+ \nu_\tau}$ can be improved to be $(5.34 \pm 0.13) \times 10^{-2}$. Using the world average of $\mathcal{B}_{D_s^+ \rightarrow \mu^+ \nu_\mu}$ [2], the ratio of the BFs is determined to be $\mathcal{B}_{D_s^+ \rightarrow \tau^+ \nu_\tau} / \mathcal{B}_{D_s^+ \rightarrow \mu^+ \nu_\mu} = 9.72 \pm 0.37$, which is consistent with the SM prediction 9.75 ± 0.01 .

In summary, with data samples corresponding to an integrated luminosity of 6.32 fb^{-1} collected at center-of-mass energies between 4178 and 4226 MeV, we present a precise measurement of the absolute branching fraction for $D_s^+ \rightarrow \tau^+ \nu_\tau$. The precision is improved by a factor of two compared to the previous best result [17]. Taking inputs from the SM global CKM fit and LQCD separately, the decay constant $f_{D_s^+}$ and the magnitude of the CKM matrix element $|V_{cs}|$ are also extracted individually; each are the most precise results to date. Combining our result with the world average $\mathcal{B}_{D_s^+ \rightarrow \tau^+ \nu_\tau}$ and $\mathcal{B}_{D_s^+ \rightarrow \mu^+ \nu_\mu}$, we test the LFU in τ - μ flavors, and no LFU violation is found with the current precision.

ACKNOWLEDGMENTS

The BESIII collaboration thanks the staff of BEPCII and the IHEP computing center for their strong support. This work is supported in part by National Key R&D Program of China under Contracts Nos. 2020YFA0406400, 2020YFA0406300; National Natural Science Foundation of China (NSFC) under Contracts Nos. 11805037, 11875054, 11625523, 11635010, 11735014, 11822506, 11835012, 11875122, 11935015, 11935016, 11935018, 11961141012, 12022510, 12025502, 12035009, 12035013, 12061131003; the Chinese Academy of Sciences (CAS) Large-Scale Scientific Facility Program; Joint Large-Scale Scientific Facility Funds of the NSFC and CAS under Contracts Nos. U1832121, U1732263, U1832207; CAS Key Research Program of Frontier Sciences under Contract No. QYZDJ-SSW-SLH040; 100 Talents Program of CAS; INPAC and Shanghai Key Laboratory for Particle Physics and Cosmology; Excellent Youth Foundation of Henan Province No. 212300410010; The youth talent support program of Henan Province No. ZYQR201912178; The Program for Innovative Research Team in University of Henan Province No. 19IRTSTHN018; ERC under Contract No. 758462; European Union Horizon 2020 re-

search and innovation programme under Contract No. Marie Skłodowska-Curie grant agreement No 894790; German Research Foundation DFG under Contracts Nos. 443159800, Collaborative Research Center CRC 1044, FOR 2359, FOR 2359, GRK 214; Istituto Nazionale di Fisica Nucleare, Italy; Ministry of Development of Turkey under Contract No. DPT2006K-120470; National Science and Technology fund; Olle Engkvist Foundation under Contract No. 200-0605; STFC (United Kingdom); The Knut and Alice Wallenberg Foundation (Sweden) under Contract No. 2016.0157; The Royal Society, UK under Contracts Nos. DH140054, DH160214; The Swedish Research Council; U. S. Department of Energy under Contracts Nos. DE-FG02-05ER41374, DE-SC-0012069.

-
- [1] D. Silverman and H. Yao, *Phys. Rev. D* **38**, 214 (1988).
- [2] P. A. Zyla *et al.* (Particle Data Group), *Prog. Theor. Exp. Phys.* **2020**, 083C01 (2020).
- [3] J. P. Lees *et al.* (BABAR Collaboration), *Phys. Rev. Lett.* **109**, 101802 (2012).
- [4] J. P. Lees *et al.* (BABAR Collaboration), *Phys. Rev. D* **88**, 072012 (2013).
- [5] R. Aaij *et al.* (LHCb Collaboration), *Phys. Rev. Lett.* **113**, 151601 (2014).
- [6] R. Aaij *et al.* (LHCb Collaboration), *Phys. Rev. Lett.* **115**, 111803 (2015).
- [7] S. Wehle *et al.* (Belle Collaboration), *Phys. Rev. Lett.* **118**, 111801 (2017).
- [8] S. Fajfer, I. Nisandzic, and U. Rojec, *Phys. Rev. D* **91**, 094009 (2015).
- [9] S. Aoki *et al.* (Flavour Lattice Averaging Group), *Eur. Phys. J. C* **80**, 113 (2020).
- [10] K. M. Ecklund *et al.* (CLEO Collaboration), *Phys. Rev. Lett.* **100**, 161801 (2008).
- [11] P. U. E. Onyisi *et al.* (CLEO Collaboration), *Phys. Rev. D* **79**, 052002 (2009).
- [12] J. P. Alexander *et al.* (CLEO Collaboration), *Phys. Rev. D* **79**, 052001 (2009).
- [13] P. Naik *et al.* (CLEO Collaboration), *Phys. Rev. D* **80**, 112004 (2009).
- [14] P. del Amo Sanchez *et al.* (BABAR Collaboration), *Phys. Rev. D* **82**, 091103(R) (2010).
- [15] A. Zupanc *et al.* (Belle Collaboration), *J. High Energy Phys.* **09**, 139 (2013).
- [16] M. Ablikim *et al.* (BESIII Collaboration), *Phys. Rev. D* **94**, 072004 (2016).
- [17] M. Ablikim *et al.* (BESIII Collaboration), [arXiv:2102.11734 \[hep-ex\]](https://arxiv.org/abs/2102.11734).
- [18] M. Ablikim *et al.* (BESIII Collaboration), [arXiv:2105.07178 \[hep-ex\]](https://arxiv.org/abs/2105.07178).
- [19] Throughout this Letter, charge conjugate channels are implied.
- [20] The E_{cm} measurement is described in M. Ablikim *et al.* (BESIII Collaboration), *Chin. Phys. C* **40**, 063001 (2016), which includes the result for the data sample at $E_{\text{cm}} =$ around 4226 MeV. The E_{cm} values for the other data samples have been obtained by a similar procedure.
- [21] The integrated luminosity measurement is described in M. Ablikim *et al.* (BESIII Collaboration), *Chin. Phys. C* **39**, 093001 (2015), which includes the result for the data sample at $E_{\text{cm}} =$ around 4226 MeV. The integrated luminosity values for the other data samples have been obtained by a similar procedure.
- [22] M. Ablikim *et al.* (BESIII Collaboration), *Nucl. Instrum. Meth. A* **614**, 345 (2010).
- [23] M. Ablikim *et al.* (BESIII Collaboration), *J. High Energy Phys.* **08**, 146 (2020).
- [24] C. H. Yu *et al.*, Proceedings of IPAC2016, Busan, Korea, 2016, [doi:10.18429/JACoW-IPAC2016-TUYA01](https://doi.org/10.18429/JACoW-IPAC2016-TUYA01).
- [25] S. Agostinelli *et al.* (GEANT4 Collaboration), *Nucl. Instrum. Meth. A* **506**, 250 (2003).
- [26] R. M. Baltrusaitis *et al.* (MARK-III Collaboration), *Phys. Rev. Lett.* **56**, 2140 (1986).
- [27] J. Adler *et al.* (MARK-III Collaboration), *Phys. Rev. Lett.* **60**, 89 (1988).
- [28] M. Ablikim *et al.* (BESIII Collaboration), *Phys. Rev. Lett.* **122**, 071802 (2019).
- [29] M. Ablikim *et al.* (BESIII Collaboration), *Chin. Phys. C* **37**, 123001 (2013); *Phys. Lett. B* **753**, 629 (2016).
- [30] M. Ablikim *et al.* (BESIII Collaboration), *Phys. Rev. Lett.* **122**, 061801 (2019).
- [31] M. Ablikim *et al.* (BESIII Collaboration), *Phys. Rev. Lett.* **122**, 121801 (2019).
- [32] M. Ablikim *et al.* (BESIII Collaboration), *Phys. Rev. D* **94**, 112003 (2016).
- [33] J. Hietala, D. Cronin-Hennessy, T. Pedlar, and I. Shipsey, *Phys. Rev. D* **92**, 012009 (2015).
- [34] M. Ablikim *et al.* (BESIII Collaboration), *Phys. Rev. D* **97**, 012006 (2018).
- [35] B. Aubert *et al.* (BABAR Collaboration), *Phys. Rev. D* **78**, 051101 (2008).
- [36] K. M. Ecklund *et al.* (CLEO Collaboration), *Phys. Rev. D* **80**, 052009 (2009).
- [37] M. Ablikim *et al.* (BESIII Collaboration), [arXiv:2104.07311 \[hep-ex\]](https://arxiv.org/abs/2104.07311).
- [38] M. Ablikim *et al.* (BESIII Collaboration), *Phys. Rev. D* **89**, 051104(R) (2014).